Nuclear Physics **A453** (1986) 58-76

LOW-ENERGY COLLECTIVE E1 MODE IN NUCLEI

G.A. LEANDER

UNISOR, Oak Ridge Associated Universities, Oak Ridge, Tennessee USA

W. NAZAREWICZ[1]

Joint Institute for Heavy-Ion Research, Oak Ridge, Tennessee, USA

G.F. BERTSCH[2]

Oak Ridge National Laboratory, Oak Ridge, Tennessee, USA

J. DUDEK

Centre de Recherches Nucléaires, F-67037 Strasbourg, France

Received 5 November 1985

Abstract: A theory is formulated for the collective enhancement of low-energy E1 transitions that has been observed in certain nuclei. The idea is to calculate an adiabatic isovector as well as isoscalar deformation. When this theory is applied to radium and light thorium nuclei, shell effects on the isovector E1 moment are found to explain the peculiar systematics of the E1 mode in this region.

1. Introduction

The nucleus cannot have a significant electric dipole (E1) moment, since the parity of any nuclear state is very nearly conserved. However, this statement is true only in the laboratory frame. Many successes of nuclear theory have been attained by working in an intrinsic frame, whose orientation is defined by the instantaneous shape of the nuclear mass distribution [1]). A large E1 moment may arise in the intrinsic frame of reference, provided that the shape has reflection asymmetry which breaks the intrinsic parity. Such an intrinsic E1 moment would be manifested by collective E1 transitions within rotational bands. This was understood early on by Strutinsky [2]) and by Bohr and Mottelson [3]), who however derived conflicting expressions for the E1 moment as a function of the nuclear shape. Strutinsky's derivation is the one that is technically correct, and qualitatively it is in fact empirically confirmed in the present work. However, this early work pertains to the liquid-drop model alone. Recently it has been plausibly demonstrated that the same kind of valence shell effects, which are crucial to the isoscalar deformation of the nucleus, also influence the isovector E1 deformation by an amount typically of the

[1] Permanent address: Institute of Physics, Technical University of Warsaw, Warsaw, Poland.

[2] Present address: Department of Physics, Michigan State University, East Lansing, Michigan 48824, USA.

same magnitude as the liquid-drop effect [4]). Since the shell effect may either cancel or enhance the liquid-drop effect, very different E1 moments can occur in nuclei of similar, reflection-asymmetric shape.

The first objective of this paper is to formulate a theory by which the intrinsic E1 moment can be calculated for an arbitrary deformed nucleus, along the same lines as a calculation of the intrinsic quadrupole moment. This theory is then tested numerically on the doubly-even nuclei of the Ra–Th region. Intrinsic reflection-asymmetric deformations have been established in these nuclei both theoretically and by numerous experiments [see e.g. refs. [5–7])], and cases of strong E1 enhancement were discovered experimentally a few years ago [8,9]).

In ^{218}Ra, a strongly collective in-band E1 decay mode was discovered experimentally by Fernandez-Niello *et al.* [8]), and subsequently several neighboring isotopes were found to have this feature. On the other hand, in ^{224}Ra, which is one of the best candidates for stable reflection asymmetry, it had previously been found by Kurcewicz *et al.* [10]) that the E1 transitions are weak. E1 shell effects will explain this anomaly.

A different theoretical approach to the E1 transition rates than the present deformed-shell-model theory is the vibron model of ref. [11]). The variation of the E1 rates in the Ra isotopes has been parametrized but not yet explained within this model.

2. Method for calculating E1 moments

Nuclear densities are well described by independent nucleons in a common potential field. There are two strategies for choosing that potential. One is to calculate it from the Hartree–Fock theory of an effective hamiltonian. The other, which we apply, is to separate average contributions to various properties from quantal fluctuations, following Strutinsky [12,13]). This allows us to simplify the potential model for calculating the fluctuations. In the Strutinsky method, the E1 moment of a nucleus will have an average part, associated with the shape variables of the nucleus, as well as a shell fluctuation. If the potential field were taken to be purely isoscalar, there would be no average contribution to an isovector E1 moment, and all of the moment would be in the shell fluctuation part. However, the isovector components of the potential, namely the Coulomb field and the isovector nuclear potential, are actually very important in determining the E1 moments. The Coulomb field makes a definite average contribution depending on the higher-multipolarity isoscalar deformations. It is derived from the semi-empirical liquid-drop model, as described in subsect. 2.1. The isovector nuclear field contribution to the average E1 moment will be automatically included by the method. Its contribution to shell fluctuation will be treated as a renormalization, and is discussed in subsect. 2.2. Thus, making the Strutinsky separation, the E1 moment for a given shape $\{\beta_i\}$ of the nucleus is written as the sum of a liquid-drop term and a renormalized shell correction from

the single-particle model:

$$Q_1(\{\beta_i\}) = Q_1^{\mathrm{LD}}(\{\beta_i\}) + Q_1^{\mathrm{SC}}(\{\beta_i\}) . \tag{2.1}$$

The E1 moment of a given configuration of the nucleus, for example the ground state, is evaluated at the deformation $\{\beta_i\}$ which minimizes the energy, which latter is also obtained by the Strutinsky renormalization method. Formulas for Q_1^{LD} and Q_1^{SC} are obtained below (eqs. (2.6–12) and (2.15)).

2.1. THE LIQUID-DROP E1 MOMENT

The bulk properties of the nucleus are represented by the liquid-drop model. A two-fluid neutron–proton liquid drop will acquire an E1 moment if the surface of the drop has a reflection asymmetric shape, e.g. when $\beta_3 \neq 0$ with the standard parametrization of the surface

$$R = R_0\left(1 + \sum_{l=1}^{\infty} \beta_1 Y_{l0}\right) . \tag{2.2}$$

The local volume polarization of electric charge can be derived from the requirement of a minimum in the energy functional [see e.g. ref. [14])]. It is

$$\frac{\rho_{\mathrm{p}} - \rho_{\mathrm{n}}}{\rho_{\mathrm{p}} + \rho_{\mathrm{n}}} = -\frac{1}{4C}\, \mathrm{e}V_{\mathrm{C}}(\mathbf{r}) , \tag{2.3}$$

where ρ_{p} and ρ_{n} are the proton and neutron densities, C is the volume symmetry-energy coefficient of the liquid-drop model, and V_{C} is the Coulomb potential generated by ρ_{p}. To lowest order,

$$V_{\mathrm{C}}(\boldsymbol{r}) = \frac{eZ}{R_0}\left(\frac{3}{2} - \frac{1}{2}\left(\frac{r}{R_0}\right)^2 + \sum_{l=1}^{\infty} \frac{3}{2l+1}\left(\frac{r}{R_0}\right)^l \beta_l\, Y_{l0}\right) . \tag{2.4}$$

It is a straightforward exercise to calculate the E1 moment,

$$Q_1^{\mathrm{LD}} = e \int z \rho_{\mathrm{p}}\, \mathrm{d}\tau , \tag{2.5}$$

by using these relations, keeping the center of gravity fixed at $z = 0$ by an appropriate choice of β_1, and retaining the lowest-order terms in the β_l's. The result is

$$Q_1^{\mathrm{LD}} = C_{\mathrm{LD}} AZe\left(\beta_2\beta_3 + \frac{88}{27\sqrt{5}}\beta_3\beta_4 + \cdots\right) , \tag{2.6}$$

where

$$C_{\mathrm{LD}} = \frac{9}{56\sqrt{35}}\frac{e^2}{\pi C} .$$

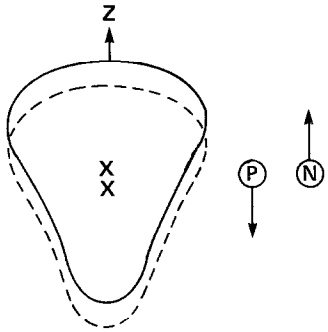

Fig. 1. Schematic picture of the displacement between the neutron and proton centers of mass due to Coulomb volume polarization in a liquid drop with octupole deformation ($\beta_3 < 0$ or $\varepsilon_3 > 0$).

The $\beta_2\beta_3$ term in eq. (2.6) is the one obtained by Strutinsky [2]). Physically, this term arises because the protons move toward the pointed end of the nuclear pear shape, like electrons on a conductor (fig. 1). The $\beta_3\beta_4$ term is about as large as the $\beta_2\beta_3$ term for light Ra–Th nuclei and thus should not be neglected. Strutinsky's numerical estimate of C_{LD} is 0.00069 fm, obtained from the Fermi gas value of the symmetry-energy coefficient, $C = 18$ MeV. Empirical mass formulas have values of C up to twice as large [15]), however, which implies a corresponding reduction of C_{LD}. Another uncertainty in Q_1^{LD} stems from the neglect of surface effects. A recent investigation of the droplet model has even indicated that the surface terms nearly cancel the volume terms for shapes corresponding to the light Ra–Th nuclei [16]). In the numerical calculations below we find that an *ad hoc* value about 15% below Strutinsky's value,

$$C_{\mathrm{LD}} = 0.00060 \text{ fm}, \tag{2.7}$$

leads to overall agreement between theory and experiment.

2.2. THE SHELL CORRECTION TO THE E1 MOMENT

Quantal effects to be superposed on the liquid drop may be derived from the single-particle states in a one-body potential [12,13]). In the present case, it is also necessary to take into account that residual interaction between the single-particle states, which depletes the E1 strength of low-lying nuclear states and puts it in the giant E1 resonance.

For the single-particle potential we have used the Woods–Saxon potential specified below in sect. 3. The shell correction for pure single-particle states is obtained as the sum over the occupied proton states of the mean deviation from the center of mass,

$$Q_1^{\mathrm{SP}} = e\frac{N}{A}\langle z_{\mathrm{p}}\rangle - e\frac{Z}{A}\langle z_{\mathrm{n}}\rangle, \tag{2.8}$$

minus an average value obtained by smoothing this sum as a function of particle number,

$$\tilde{Q}_1^{\mathrm{SP}} = \mathrm{e}\frac{N}{A}\langle \tilde{z}_\mathrm{p}\rangle - e\frac{Z}{A}\langle \tilde{z}_\mathrm{n}\rangle . \tag{2.9}$$

In eq. (2.8),

$$\langle z\rangle = \sqrt{\tfrac{4}{3}\pi}\sum_i \langle i|rY_{10}|i\rangle v_i^2 , \tag{2.10}$$

where v_i^2 is the BCS occupation coefficient for the state i. The smoothed value $\langle \tilde{z}\rangle$ in eq. (2.9) is defined by

$$\langle \tilde{z}\rangle = \sqrt{\tfrac{4}{3}\pi}\sum_i \langle i|rY_{10}|i\rangle n_i , \tag{2.11}$$

where n_i are the smoothed occupation numbers for the single-particle levels obtained within the Strutinsky approach [see e.g. ref. [17])]. In the presence of rotation the formula (2.10) has to be modified:

$$\langle z\rangle = \sqrt{\tfrac{4}{3}\pi}\sum_{ij} \langle i|rY_{10}|j\rangle \rho_{ij} , \tag{2.12}$$

where ρ_{ij} is the single-particle density matrix defined as $\rho_{ij} = \langle \mathrm{vac}|c_i^+ c_j|\mathrm{vac}\rangle$, and $|\mathrm{vac}\rangle$ is the HFBC vacuum [see e.g. ref. [18])].

In numerical applications to Ra–Th nuclei it turned out that the smoothed part of the single-particle E1 moment, $\tilde{Q}_1^{\mathrm{SP}}$, is accurately reproduced by the liquid-drop formula (2.6) if the numerical coefficient of the latter formula is taken to be $\tilde{C}_{\mathrm{LD}} = 0.00037$ fm. Since the Woods–Saxon proton and neutron single-particle potentials are defined to have the same center of mass, these non-zero values of $\tilde{Q}_1^{\mathrm{SP}}$ reflect the effect of the spin-orbit potential and the Coulomb term in the single-particle model [19]). The fact that the deformation dependence of $\tilde{Q}_1^{\mathrm{SP}}$ is found numerically to coincide with that of eq. (2.6) provides some further justification for the use of this functional form in connection with Q_1^{LD}.

The residual interaction which renormalizes the E1 moments relative to the single-particle model has been studied extensively in connection with the E1 giant resonance. It can be simulated by an attractive dipole-dipole interaction

$$v_{12} = \kappa \boldsymbol{d}_1 \cdot \boldsymbol{d}_2 \tag{2.13}$$

with a phenomenological strength $\kappa < 0$. A simple estimate for the screening of E1 moments due to correlations can be obtained using the random-phase approximation (RPA) treatment of v_{12} which is described in subsect. 6.5b of ref. [20]). For simplicity it is assumed that the particle–hole energy of single-particle excitations induced by the dipole operator is exactly $\hbar\omega_0$. Dipole moments including screening due to the correlations are then given, relative to the single-particle dipole moments, by

$$Q_1 = Q_1^{\mathrm{SP}} \Big/ \left(1 - \frac{2\kappa Q_{\mathrm{GR}}^2 \omega_0}{\omega_0^2 - \omega^2}\right), \tag{2.14}$$

where Q_{GR} is the transition moment to the giant resonance and $\hbar\omega$ is the transition energy with which Q_1 is associated.

The giant resonance is known empirically to lie around a frequency of $\omega_{GR} \approx 1.9\omega_0$. The requirement of a maximum at $\omega = \omega_{GR}$ on the right-hand side of eq. (2.11) - which actually becomes a divergence under the present approximations - determines the value of κQ_{GR}^2 as $-1.3\omega_0$. Finally, setting $\omega = 0$ in eq. (2.11) to obtain the ground-state E1 moment gives $Q_1 = Q_1^{SP}/3.6$. The shell correction to the E1 moment becomes

$$Q_1^{SC} = (Q_1^{SP} - \tilde{Q}_1^{SP})/3.6\,. \tag{2.15}$$

In principle, an improved estimate of the screening might be obtained by numerical solution of the RPA equation using the dipole response function of the deformed single-particle model, but it would then be necessary to have a correspondingly accurate estimate of the strength κ and its deformation dependence in order to warrant this effort. The effect of rotation on the screening is expected to be small at a given shape since the centroid of the giant dipole resonance depends primarily on deformation [21]).

3. Calculations

Realistic calculations have been carried out for the doubly-even Ra and Th isotopes. Rotation of the nucleus has been included since much of the available experimental data is for high-spin states. The first step of the calculation is to determine the equilibrium shapes at the appropriate angular momenta, and the second step is to determine the E1 moments at the equilibrium shapes.

Both steps are carried out by the Strutinsky renormalization method. The liquid-drop energy functional is the one in ref. [22]), and the liquid-drop E1 polarization is described in subsect. 2.1 above. The shell correction is obtained from the single-particle states in the deformed and rotating Woods-Saxon potential of ref. [23]), with the "universal" single-particle parameter set of ref. [24]). The Strutinsky smoothing is carried out with standard parameters, namely a value of $1.2 \times 41 A^{-1/3}$ MeV for the smoothing range γ, and order $p = 6$ for the correction polynomial [17]). A superfluid pair field is included using the parameters of ref. [25]), but for non-zero spins the gap parameter is determined by a simplified procedure as compared to full self-consistency [see ref. [26])].

The general form of the Strutinsky energy functional including rotation and pairing is described e.g. in ref. [27]). Equilibrium shapes for Ra and Th nuclei resulting from the minimization of this energy functional will be presented and discussed in detail in a separate paper [26]). The main features are as follows. Some lighter isotopes, ^{218,220}Ra and ^{220}Th, have spherical ground states but acquire octupole along with quadrupole and hexadecapole deformation in the yrast rotational states all the way up to very high spins. The heavier isotopes $^{222-226}$Ra and $^{222-228}$Th each have their

own roughly constant deformation, including an octupole component, throughout the known part of the yrast band. At somewhat higher spins in these heavier isotopes, a band with about the same β_2 and β_4 deformation but with no reflection asymmetric β_3 deformation is predicted to cross the yrast line.

The present results on E1 moments at the equilibrium shapes are compared with experiment in sect. 4 below. The remainder of this section describes some "numerical experiments" that may help to clarify the significance of the calculated values. Results from the first of these numerical exercises are shown in fig. 2, which gives the difference $\langle z\rangle - \langle \tilde{z}\rangle$ (eqs. (2.10, 11)) for protons and neutrons separately. The deformation is held fixed for all particle numbers. The overall particle-number dependence does not depend much on which deformation is chosen. Fig. 2 illustrates two features. Firstly, the quantal fluctuations of the dipole moment are collective in nature, following a systematic trend through the major shell and not just fluctuating randomly from one single-particle orbital to the next. The collectivity obviously

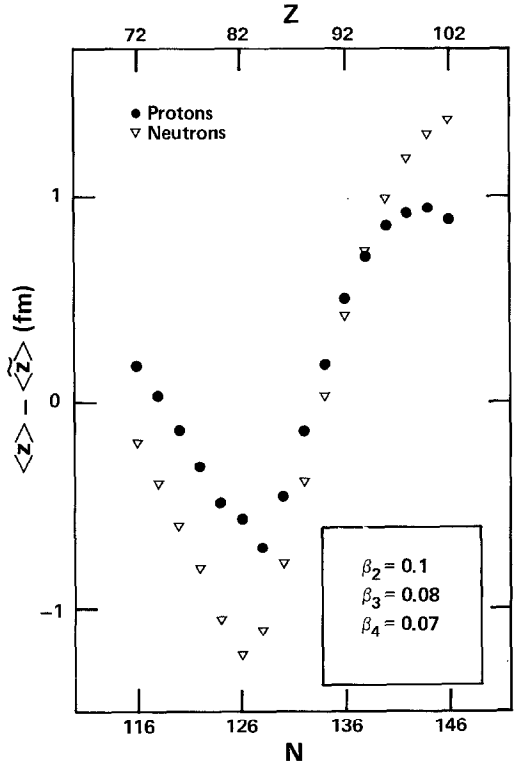

Fig. 2. The Strutinsky-renormalized displacement of the center of mass in an octupole deformed single-particle potential as a function of the number of particles filling the lowest orbits, for protons (filled circles, upper axis) and neutrons (open triangles, lower axis). Note the coherent contributions from orbits just above the $Z = 82$ and $N = 126$ shell gaps.

enhances the maximum deviation of the shell correction from its average. Coherence between the dipole and octupole moments on the microscopic level has interestingly been noted also in the context of a different model [28]). Secondly, since the E1 moment is a weighted difference between the proton and neutron dipole moments (eq. (2.8)), the E1 shell correction can be expected to increase with increasing Z and decreasing N in the Ra–Th region. This trend is in fact borne out qualitatively by the experimental data [4]).

Figs. 3a and b show the E1 shell correction as a function of β_2 and β_3 deformation at fixed particle number. Note that the overall topology of the surfaces is rather similar in figs. 3a and b. Thus it is the general trend revealed by fig. 2, in combination with the effect of deformation changes on this topography, that governs the dependence of the E1 shell correction on particle number. The effect of angular momentum on plots like figs. 3a and b is generally small. Only rarely does the occupation of aligned quasiparticle orbits *per se* give an observable change of the E1 shell correction. However, given that figs. 3a and b are roughly independent of angular momentum, it is evident from the close spacing of contour lines in some places that deformation changes induced by rotation can have a significant effect. Thus E1 transition rates could in principle serve as a sensitive probe of deformation changes at high spin.

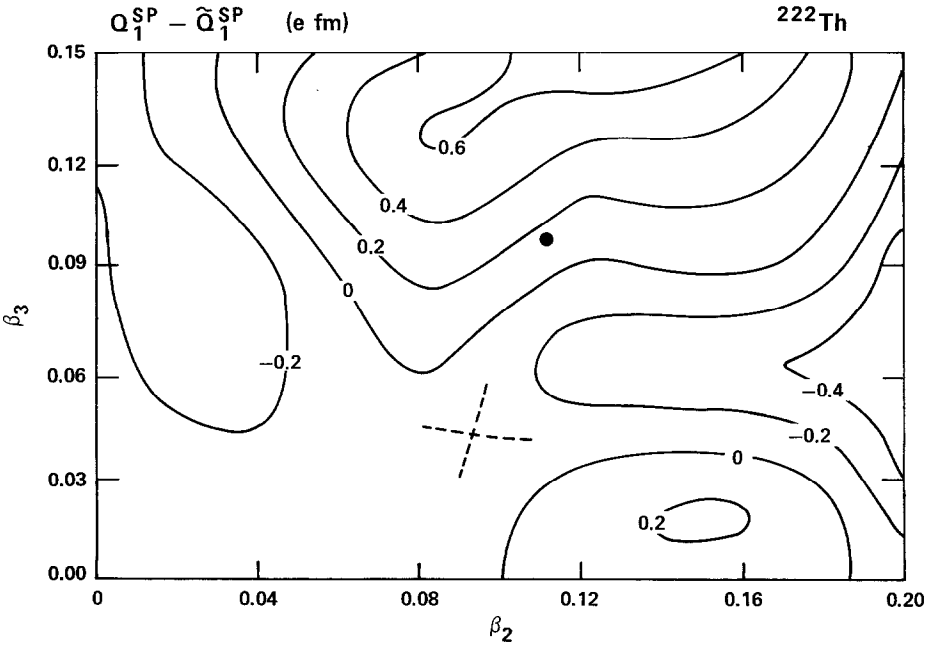

Fig. 3a. The single-particle E1 moment after Strutinsky renormalization, $Q_1^{SP} - \tilde{Q}_1^{SP}$, plotted versus β_2 and β_3 for ^{222}Th. The solid circle marks the calculated equilibrium shape of ^{222}Th. note the sensitivity of the E1 moment to the equilibrium shape.

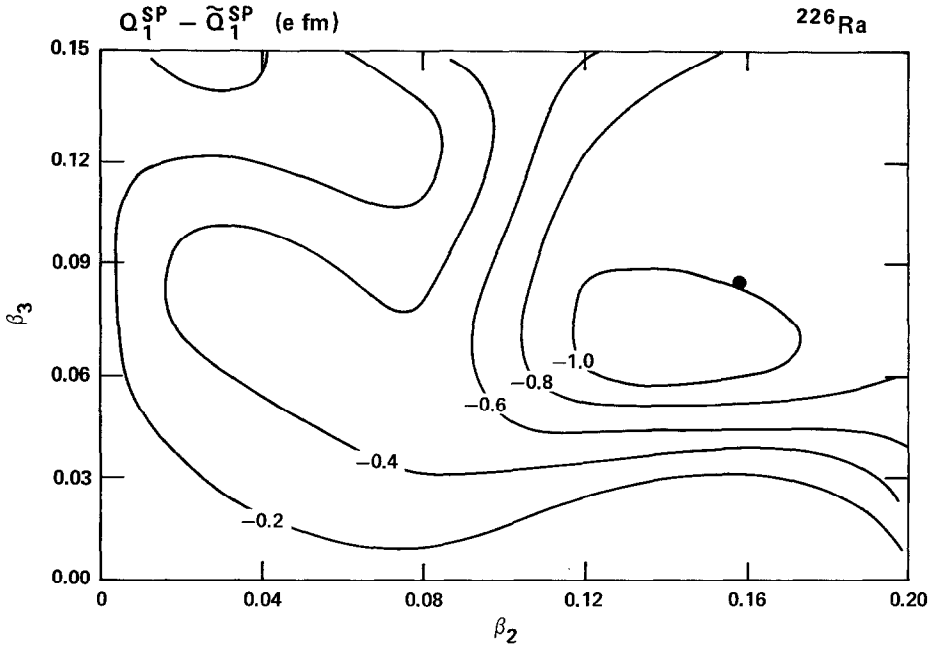

Fig. 3b. Same as fig. 3a, but for ^{226}Ra.

4. Comparison with experiment

For the axial shapes considered in this work (eq. (2.2)), the isoscalar deformation leads to rotational bands of alternating parity. The isovector E1 deformation leads to collective E1 transitions, in-band between the states of opposite parity (fig. 4). The selection rules for quasiparticle transitions are less obvious and are derived below in the appendix. Experimental information on E1 moments is mainly available from $B(\mathrm{E1})/B(\mathrm{E2})$ branching ratios, since lifetime measurements have been made only in some isolated cases [32,33]). The extraction of moments from these ratios assumes that intrinsic moments can be related to the reduced transition rates via the rotational model [20]):

$$B(\mathrm{E1}) = \frac{3}{4\pi} Q_1^2 \langle I_i K 10 | I_f K \rangle^2 , \tag{4.1}$$

$$B(\mathrm{E2}) = \frac{5}{16\pi} Q_2^2 \langle I_i K 20 | I_f K \rangle^2 . \tag{4.2}$$

Theoretical quadrupole moments Q_2 are obtained from the calculated equilibrium shapes. The shell correction to Q_2 is insignificant because the isoscalar deformation is chosen to minimize the Strutinsky energy, and this is approximately equivalent to achieving Hartree–Fock self-consistency [12,13,19]). It may be noted that the leading

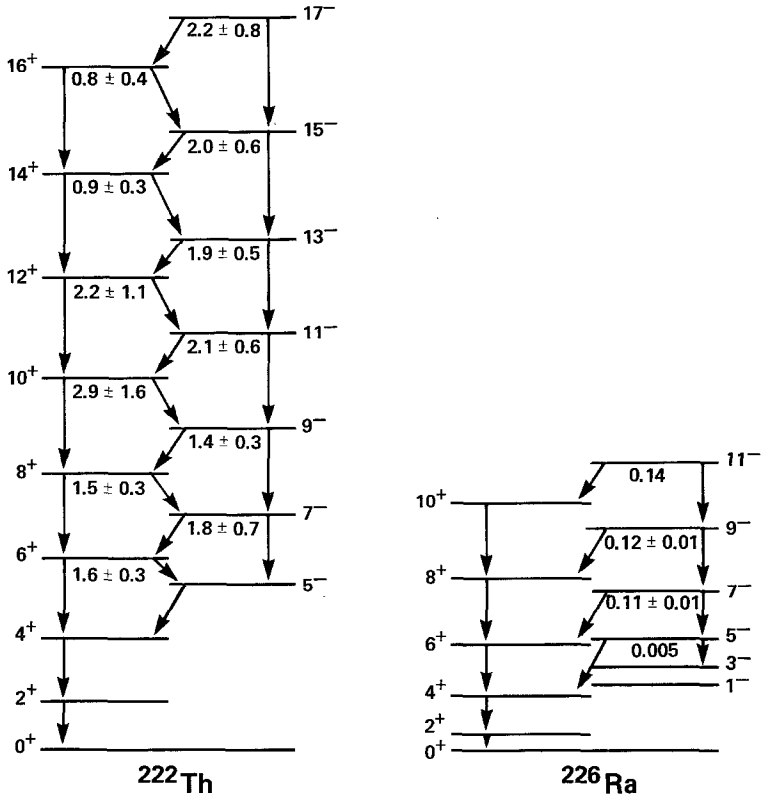

Fig. 4. Experimental [29-31]) yrast bands of ^{222}Th and ^{226}Ra. A number below a level is the $B(E1)/B(E2)$ branching ratio for that level in 10^{-6} fm^{-2}.

liquid-drop term in eq. (2.6) is proportional to β_2, so if all other contributions are neglected the $B(E1)/B(E2)$ ratio becomes independent of the quadrupole moment, Q_2.

4.1. THE Ra AND Th NUCLEI

The most salient feature of the E1 moments from experiment is that they are an order of magnitude larger in the lighter octupole deformed Ra and Th isotopes than in the heavier ones [e.g. ref. [34]), fig. 4 and table 1 below]. The explanation which emerges from the present theory is that in the light isotopes the liquid-drop contribution and the shell correction to the E1 moment have the same sign and add coherently, but in the heavy isotopes they have opposite signs and nearly cancel. A quantitative illustration of this is provided in figs. 5a and b. The upper part of each figure shows the Strutinsky energy, plotted as a function of β_3 after minimization with respect to β_2 and β_4.

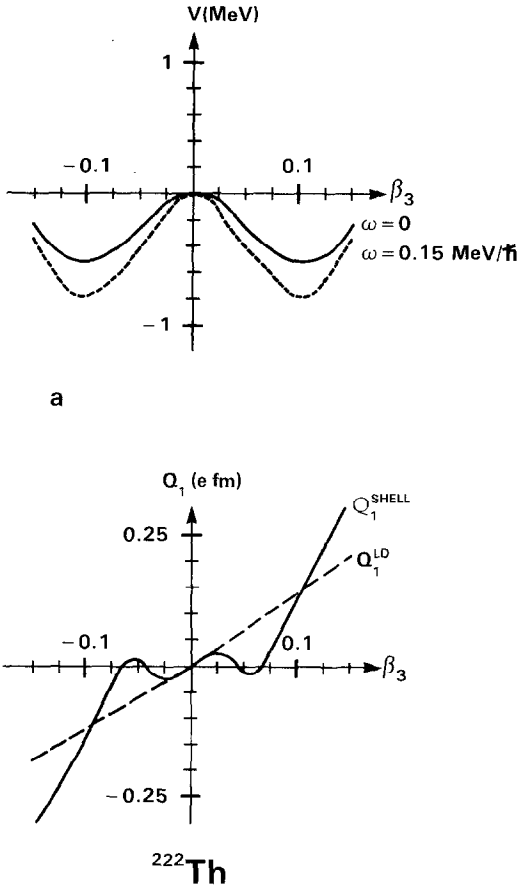

Fig. 5a. The potential energy of ^{222}Th (upper plot) at two rotational frequencies ω, and the two terms of eq. (2.1) (lower plot) whose sum is the E1 moment Q_1. They are plotted along the minimum potential energy valley of the β_3 shape coordinate. The two terms in Q_1 have the same sign and add coherently at the potential energy minimum, $\beta_3 \approx 0.1$ or -0.1.

The lower parts of figs. 5a and b show the liquid-drop and shell contributions to the E1 moment. For the two nuclei shown, ^{222}Th and ^{226}Ra, these curves are not very sensitive to rotation in the spin region of interest. At the equilibrium deformation of ^{222}Th the liquid-drop and shell terms enhance each other. The precise value of the coefficient of the liquid-drop term, quoted in subsect. 2.1 and used in fig. 5, was in fact adjusted so as to reproduce the experimental $B(\mathrm{E1})/B(\mathrm{E2})$ ratio [29]), 2×10^{-6} fm^{-2}, in ^{222}Th. This value of the coefficient was then used throughout, and in particular for ^{226}Ra it is seen in fig. 5b that a near perfect cancellation results between the liquid-drop and shell terms at the equilibrium deformation, thereby explaining a reduction of the experimental $B(\mathrm{E1})/B(\mathrm{E2})$ ratio by one to two orders of magnitude relative to ^{222}Th (fig. 4).

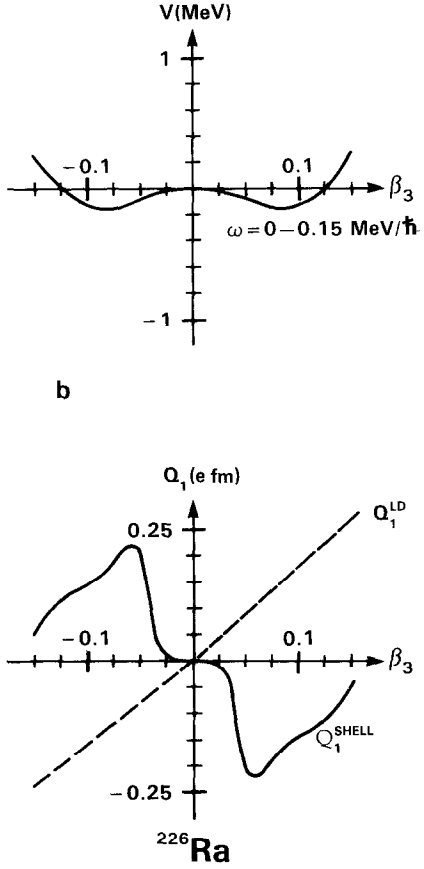

Fig. 5b. Same as fig. 5a, but for ^{226}Ra. At the potential energy minimum the two terms in Q_1 have opposite signs and cancel.

A comparison between theory and the available data on doubly-even Ra-Th nuclei is displayed in table 1, along with predictions for those nuclei where $B(\mathrm{E1})/B(\mathrm{E2})$ ratios have not yet been measured. Good agreement is found between theoretical and experimental $B(\mathrm{E1})/B(\mathrm{E2})$ ratios. The level of numerical agreement is perhaps "too good", considering that the small ratios result from the cancellation of two large numbers, and that the large ratios occur in transitional nuclei where the effective dynamical shape may differ from the static equilibrium shape used here.

Let us now consider the angular momentum dependence of the $B(\mathrm{E1})/B(\mathrm{E2})$ ratios. Experimentally, a definite trend can be discerned through the error bars in ^{226}Ra and ^{222}Th. In ^{226}Ra, the $B(\mathrm{E1})/B(\mathrm{E2})$ ratio increases with increasing spin (fig. 4), but is still small at the highest spin, $I = 11\hbar$. An explanation does not emerge explicitly from the present calculation but is suggested by fig. 5b. The potential-energy curve in the upper part of fig. 5b is almost flat, and it appears plausible that rotation might shift the effective deformation a little bit, although almost no change of the

TABLE 1

Theory versus experiment for the $B(E1)/B(E2)$ branching ratios in doubly-even Ra–Th nuclei

Nucleus	β_2	β_3	β_4	Q_t [e·fm]	Q_2 [e·b]	$\langle I \rangle$	$B(E1)/B(E2)$ [fm^{-2}]	
							theory	experiment
^{218}Ra	0.02	0.08	0.013	−0.07	0.75	12	1.1×10^{-6}	2.4×10^{-6}
	−0.06		0.037	−0.11	−2.26		5.0×10^{-6}	
^{220}Ra	0.11	0.10	0.065	0.19	4.6	4–9	9×10^{-7}	1×10^{-6}
	0.11	0.08	0.065	0.13	4.3	17	4×10^{-7}	
^{222}Ra	0.12	0.11	0.071	0.18	5.2	5–12	6×10^{-7}	
	0.13	0.04	0.076	0.17	5.3	21	8×10^{-8}	
^{224}Ra	0.14	0.11	0.081	0.12	6.0	8	2×10^{-7}	1×10^{-7}
	0.14	0.04	0.081	0	5.8	23	0	
^{226}Ra	0.16	0.09	0.090	0.05	6.8	3–11	3×10^{-8}	$<2\times10^{-7}$
	0.15	0.05	0.086	0.05	6.3	24	3×10^{-8}	
^{220}Th	0.07	0.07	0.043	0.20	2.8	13	2.5×10^{-6}	1.9×10^{-6}
^{222}Th	0.11	0.10	0.065	0.32	5.0	0–12	2.0×10^{-6}	2×10^{-6}
	0.13	0	0.076	0	5.4	26	0	
^{224}Th	0.14	0.11	0.081	0.33	5.9	5–14	1.6×10^{-6}	
^{226}Th	0.15	0.11	0.086	0.29	6.6	6	9.6×10^{-7}	4×10^{-7}
	0.15	0	0.086	0	6.6	20	0	
^{228}Th	0.18	0.08	0.099	0.10	7.7	8	9×10^{-8}	8×10^{-8}
	0.18	0	0.099	0	7.8	15	0	

Cols. 2–4 indicate the calculated equilibrium shapes. In addition, β_5 and β_6 were included according to the liquid-drop prescription of ref. [35]). Cols. 5 and 6 give the calculated electric dipole and quadrupole moments, respectively. Col. 7 shows the approximate region of angular momentum for which the other entries apply. In some cases, numbers are given for two different spin regions. Col. 8 gives the theoretical and col. 9 the experimental branching ratios in fm^{-2}. Experimental data are taken from refs. [8,10,29–31,34,36–39]). The latter have sizable uncertainties (e.g. fig. 4), especially for ^{228}Th where lines barely visible in the e-γ coincidence spectrum are assumed here to be of equal intensity.

equilibrium deformation was obtained in the present calculation. The lower part of fig. 5b shows that the E1 shell correction is highly sensitive to β_3 deformation, so that a small shift in β would disturb the near-perfect cancellation between liquid-drop and shell terms that is suggested by the very small $B(E1)/B(E2)$ ratios at low spin.

For ^{222}Th, a discernible feature of the data (fig. 4) is that the $B(E1)/B(E2)$ ratio decreases at the highest spins for positive- but not for negative-parity initial states. This could be connected with the fact that the positive- but not the negative-parity states may interact with a reflection-*symmetric* band that is predicted to cross the yrast line at $I \approx 26\hbar$.

4.2. RARE-EARTH NUCLEI

Although neither our calculations nor the experimental data are as complete in the rare-earth region as in the Ra–Th region, we can forward some qualitative considerations and relate them to available data. Reflection-asymmetric equilibrium

shapes are predicted for the ground states of the neutron-rich nuclei around ^{146}Ba [refs. [35,40])] and exclusively at very high spins for some other rare-earth nuclei [41]). Experimentally, enhanced E1 transitions have been observed in $^{148-150}$Sm [refs. [42,43])]. In these nuclei, alternating-parity bands develop above $I = 4\hbar$. The measured $B(\mathrm{E1})/B(\mathrm{E2})$ branching ratios are of the order of $10^{-6}\,\mathrm{fm}^{-2}$, which is even faster than in the Ra–Th nuclei if a scaling by $A^{2/3}$, as suggested by the liquid model, is taken into account.

Fig. 6 is similar to fig. 2 but for rare-earth nuclei. It shows the Strutinsky renormalized center-of-mass displacement obtained from the single-particle wave functions for proton numbers $48 \leq Z \leq 78$ and neutron numbers $72 \leq N \leq 102$. The general pattern in fig. 6 is the same as in fig. 2: the center-of-mass displacement exhibits long-range oscillatory behavior as a function of the shell filling, with minima at the magic numbers and maxima near the middle of the shells. The deformation parameters in fig. 6 correspond to the calculated equilibrium shape of ^{148}Sm. It is seen that for nuclei around ^{148}Sm the proton and neutron displacements have opposite signs, such that they contribute constructively with each other (eq. (2.8)) and with the liquid-drop moment to the total E1 moment. This result correlates with the large experimental $B(\mathrm{E1})/B(\mathrm{E2})$ ratios.

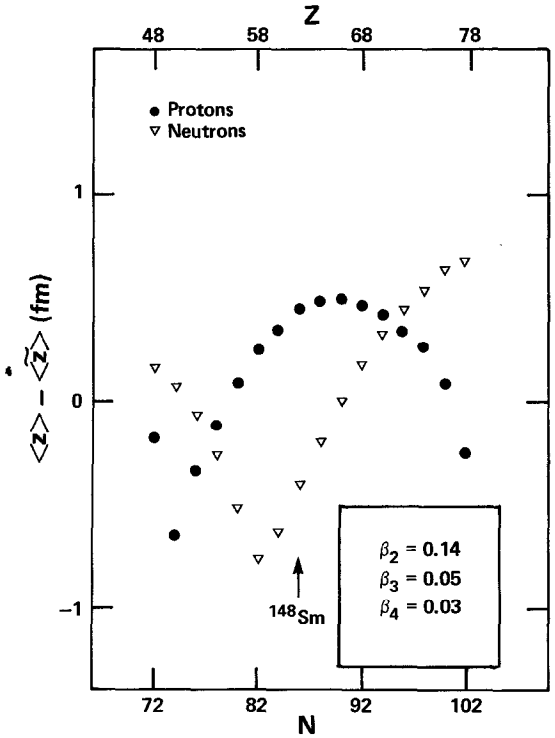

Fig. 6. Same as fig. 2, but relevant to rare-earth nuclei.

For nuclei closer to ^{146}Ba the shell correction term should become smaller, since both the proton and neutron contributions in fig. 6 are near zero for $Z \approx 56$ and $N \approx 90$. The effect of this is illustrated more quantitatively in fig. 7, which shows the E1 moments of ^{144}Ba and ^{148}Sm calculated as functions of β_3. Fig. 7 shows that a moderate octupole distortion of the order of $\beta_3 = 0.05$ in the high-spin states of ^{148}Sm would give the large E1 moment, $Q_1 \approx 0.2\, e \cdot$ fm, that would account for the experimental $B(E1)/B(E2)$ ratios of the order of 10^{-6} fm^{-2}. The $B(E1)/B(E2)$ ratios in heavy Ba nuclei are predicted to be about 4–5 times smaller.

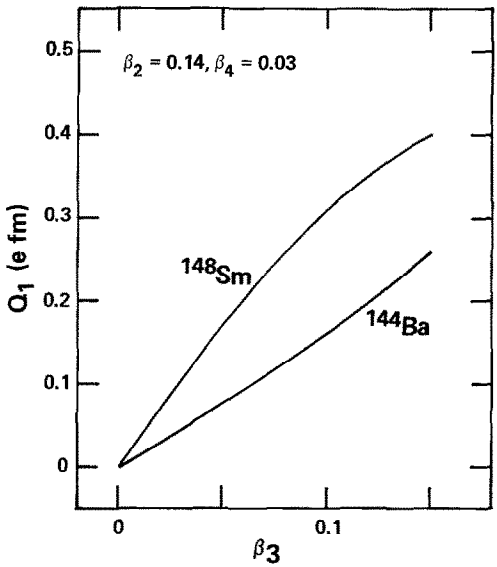

Fig. 7. Theoretical Q_1 moments (eq. (2.1)) as functions of octupole deformation for ^{148}Sm and ^{144}Ba.

5. Conclusions and discussion

A *reflection-asymmetric isoscalar* deformation is in general accompanied by an adiabatic *isovector* deformation. The isovector deformation is expected to follow the isoscalar deformation adiabatically since the frequency of the giant dipole vibrational mode is much higher than the frequency of isoscalar shape vibrations. This work shows how a static electric dipole deformation can be calculated by the Strutinsky renormalization method, taking into account the residual dipole-dipole interaction. The case of axially-symmetric shapes is treated explicitly. Such axial shapes with reflection asymmetry occur in the Ra–Th region; they are also predicted to occur in some rare-earth nuclei. Rotational bands of alternating parity, with collective E1 transitions in-band between the states of opposite parity have been observed in the Ra–Th region (table 1) and also in nuclei around ^{148}Sm.

Realistic calculations were carried out for doubly even Ra–Th nuclei. A loose end of the theory is the coefficient C_{LD} of the liquid-drop contribution to the E1 moment, which was given an *ad hoc* value within the physical range. This choice of parameter value is necessary for the high level of numerical agreement between theory and experiment in table 1. However, the trends and in particular the systematic order of magnitude difference between the lighter and heavier isotopes are an unequivocal prediction of the theory. It occurs because the shell correction tends to cancel the liquid-drop term in the heavier isotopes and increasingly enhances it in the lighter isotopes. The fast E1 transitions around ^{148}Sm also coincide with a calculated enhancement of the E1 moment by shell effects. The shell correction to the E1 moment, which thus plays a major role, is predicted to be sensitive not only to particle number but also to isoscalar shape variations, e.g. with spin, in a given nucleus.

The valuable input of Petr Vogel to this work is gratefully acknowledged. We are indebted to Christopher Lauterbach for making the data for ^{226}Ra and ^{226}Th available prior to publication. One of us (G.A.L.) extends his warmest thanks to Christopher Logothetis for fruitful and stimulating treatment at the M.D. Anderson Tumor Institute and Hospital, where this paper was completed. UNISOR is a consortium of twelve institutions, supported by them and by the Office of Energy Research of the US Department of Energy under contract no. DE-AC05-76OR0003 with Oak Ridge Associated Universities. The Joint Institute for Heavy Ion Research has as member institutions the University of Tennessee, Vanderbilt University, and the Oak Ridge National Laboratory; it is supported by the members and by the Department of Energy through contract no. DE-AS05-76ERO-4936 and DE-AC05-84OR21400 with the University of Tennessee.

Appendix

SYMMETRY PROPERTIES OF SPHERICAL TENSORS IN THE GOOD-SIMPLEX BASIS

In the presence of static octupole deformation, the rotational states of a nucleus are characterized by the simplex quantum number [44]) s, which is the eigenvalue of the simplex operator S [ref. [20])]:

$$S = PR_1^{-1} \qquad (R_\kappa = \mathrm{e}^{-i\pi j_\kappa}). \tag{A.1}$$

The Goodman transformation [45]) from the strong-coupling basis to basis states of good simplex reads [7])

$$|k, s=+i\rangle = \sqrt{\tfrac{1}{2}}(-|k, \Omega_k\rangle + (-1)^{\Omega_k - 1/2}|\overline{k, \Omega_k}\rangle)\,, \tag{A.2}$$

$$|k, s=-i\rangle=\sqrt{\tfrac{1}{2}}(|\overline{k, \Omega_k}\rangle+(-1)^{\Omega_k-1/2}|k, \Omega_k\rangle)\,, \tag{A.3}$$

where Ω is the single-particle angular momentum projection on the axis of quantization and $|\overline{k, \Omega_k}\rangle = T|k, \Omega_k\rangle$, the time-reversed state. The states of opposite simplex given by (A.2) and (A.3) can be related by means of the simplex-reversal operator [7] $U_s = -iST$:

$$|k, s\rangle = U_s|k, -s\rangle\,. \tag{A.4}$$

There exists another representation for the operator U_s. By straightforward calculation one finds

$$R_3|k, s\rangle = i|k, -s\rangle\,. \tag{A.5}$$

Thus U_s can alternatively be written in the form

$$U_s = -iR_3\,. \tag{A.6}$$

The transformation properties of spherical tensors Y_{LM} are [see eq. (A.6) and ref. [7]]:

$$U_s Y_{LM} U_s^{-1} = (-1)^M Y_{LM}\,, \tag{A7}$$

$$S Y_{LM} S^{-1} = Y_{L-M}\,. \tag{A.8}$$

In order to calculate matrix elements of the transition operators we employ eqs. (A.7) and (A.8):

$$\langle k, s|\, Y_{LM}|k', s'\rangle = (-1)^M\langle k, -s|\, Y_{LM}|k', -s'\rangle\,, \tag{A.9}$$

$$\langle k, s|\, Y_{LM}|k', s'\rangle = s^*s'(-1)^M\langle k', s'|\, Y_{LM}|k, s\rangle \tag{A.10}$$

(assuming a representation where the matrix elements are real), which implies

$$\langle k, -s|\, Y_{LM}|k', -s'\rangle = s^*s'\langle k', s'|\, Y_{LM}|k, s\rangle\,. \tag{A.11}$$

A parity doublet in an odd-mass nucleus consists of two rotational bands of opposite simplex built on states $|k, s\rangle$ and $|k, -s\rangle$.

For transitions *within* the band ($s = s'$) one obtains (eq. (A.10)

$$\langle k, s|\, Y_{LM}|k, s\rangle = (-1)^M\langle k, s|\, Y_{LM}|k, s\rangle\,, \tag{A.12}$$

which implies that

$$\langle k, s|\, Y_{LM}|k, s\rangle = 0 \qquad \text{for } M = \pm 1, \pm 3, \ldots\,. \tag{A.13}$$

For transitions between the bands ($s' = -s$), eq. (A.12) gives

$$\langle k, -s|\, Y_{LM}|k, s\rangle = -\langle k, -s|\, Y_{LM}|k, s\rangle\,, \tag{A.14}$$

which implies that

$$\langle k, -s | Y_{LM} | k, s \rangle = 0 \tag{A.15}$$

independently of the multipolarity (L, M).

References

1) A. Bohr, Mat. Fys. Medd. Dan. Vid. Selsk. **26**, no. 14 (1952)
2) V.M. Strutinsky, Atomnaya Energiya **1** (1956) 150; J. Nucl. Energy **1** (1956) 611
3) A. Bohr and B.R. Mottelson, Nucl. Phys. **4** (1957) 529; **9** (1959) 687
4) G.A. Leander, AIP Conf. Proc. **125** (American Institute of Physics, New York, 1985) 125
5) G.A. Leander, R.K. Sheline, P. Möller, P. Olanders and I. Ragnarsson, Nucl. Phys. **A388** (1982) 452
6) G.A. Leander and R.K. Sheline, Nucl. Phys. **A413** (1984) 375
7) W. Nazarewicz and P. Olanders, Nucl. Phys. **A441** (1985) 420
8) J. Fernandez-Niello, H. Puchta, F. Riess and W. Trautmann, Nucl. Phys. **A391** (1982) 221
9) I. Ahmad, J.E. Gindler, R.R. Betts, R.R. Chasman and A.M. Friedman, Phys. Rev. Lett. **49** (1982) 1758
10) W. Kurcewicz, N. Kaffrell, N. Trautmann, A. Płochocki, J. Zylicz, M. Matul and K. Stryczniewicz, Nucl. Phys. **A289** (1977) 1
11) H.J. Daley and M. Gai, Phys. Lett. **149B** (1984) 13
12) V. Strutinsky, Nucl. Phys. **A95** (1967) 420; **A122** (1968) 1
13) M. Brack, J. Damgaard, A.S. Jensen, H.C. Pauli, V.M. Strutinsky and C.Y. Wong, Rev. Mod. Phys. **44** (1972) 320
14) W.D. Myers and W.J. Swiatecki, Ann. of Phys. **55** (1969) 395
15) W.D. Myers, At. Nucl. Data Tables **17** (1976) 411
16) C.O. Dorso, W.D. Myers and W.J. Swiatecki, preprint LBL 19873, Lawrence Berkeley Laboratory, Berkeley, California (1985)
17) M. Bolsterli, E.O. Fiset, J.R. Nix and J.L. Norton, Phys. Rev. **C5** (1972) 1050
18) Z. Szymański, Fast nuclear rotation (Clarendon, Oxford, 1983)
19) J. Dudek, W. Nazarewicz and P. Olanders, Nucl. Phys. **A420** (1984) 285
20) A. Bohr and B.R. Mottelson, Nuclear structure, vol. 2 (Benjamin, Reading, Mass., 1975)
21) P. Ring, L.M. Robledo, J.L. Egido and M. Faber, Nucl. Phys. **A419** (1984) 261
22) P. Möller and J.R. Nix, Nucl. Phys. **A361** (1981) 117
23) J. Dudek, A. Majhofer, J. Skalski, T. Werner, S. Cwiok and W. Nazarewicz, J. of Phys. **G5** (1979) 1359; S. Cwiok, W. Nazarewicz, J. Dudek, J. Skalski and Z. Szymański, Nucl. Phys. **A333** (1980) 139
24) J. Dudek, Z. Szymański and T. Werner, Phys. Rev. **C23** (1981) 920
25) J. Dudek, A. Majhofer and J. Skalski, J. of Phys. **G6** (1980) 447
26) W. Nazarewicz, G.A. Leander and J. Dudek, contribution to the Symp. on electromagnetic properties of high spin states, Stockholm, 1985; Nucl. Phys. **A**, to be submitted
27) M.J.A. de Voigt, J. Dudek and Z. Szymański, Rev. Mod. Phys. **55** (1984) 949
28) I. Ahmad, R.R. Chasman, J.E. Gindler and A.M. Friedman, Phys. Rev. Lett. **52** (1984) 503
29) D. Ward, G.D. Dracoulis, J.R. Leigh, R.J. Charity, D.J. Hinde and J.O. Newton, Nucl. Phys. **A406** (1983) 591
30) W. Bonin, M. Dahlinger, S. Glienke, E. Kankeleit, M. Krämer, D. Habs, B. Schwartz and H. Backe, Z. Phys. **A310** (1983) 249
31) Ch. Lauterbach, private communication, Sept. 1985
32) M. Gai, J.F. Ennis, M. Ruscev, E.C. Schloemer, B. Shivakumar, S.M. Sterbenz, N. Tsoupas and D.A. Bromley, Phys. Rev. Lett. **51** (1983) 646
33) J. Fernandez-Niello, C. Mittag, H. Puchta, F. Riess and D. Selbmann, Univ. Munich annual report (1983), p. 51, unpublished
34) P.D. Cottle, J.F. Shriner, F. Dellagiacoma, J.F. Ennis, M. Gai, D.A. Bromley, J.W. Olness, E.K. Warburton, L. Hildingsson, M.A. Quader and D.B. Fossan, Phys. Rev. **C30** (1984) 1768
35) W. Nazarewicz, P. Olanders, I. Ragnarsson, J. Dudek, G.A. Leander, P. Möller and E. Ruchowska, Nucl. Phys. **A429** (1984) 269

36) J.D. Burrows, P.A. Butler, K.A. Connell, A.N. James, G.D. Jones, A.M.Y. El-Lawindy, T.P. Morrison, J. Simpson and R. Wadsworth, J. of Phys. **G10** (1984) 1449
37) A. Celler, Ch. Briançon, J.S. Dionisio, A. Lefebvre, Ch. Vieu, J. Zylicz, R. Kulessa, C. Mittag, J. Fernandez-Niello, Ch. Lauterbach, H. Puchta and F. Riess, Nucl. Phys. **A432** (1985) 421
38) W. Bonin, H. Backe, M. Dahlinger, S. Glienke, D. Habs, E. Hanelt, E. Kankeleit and B. Schwartz, Z. Phys. **A322** (1985) 59
39) K. Hardt, P. Schüler, C. Günther, J. Recht, K.P. Blume and H. Wilzek, Nucl. Phys. **A419** (1984) 34
40) G.A. Leander, W. Nazarewicz, P. Olanders, I. Ragnarsson and J. Dudek, Phys. Lett. **152B** (1985) 284
41) J. Dudek, W. Nazarewicz and G.A. Leander, contribution to the Niels Bohr Centennial Conf., Copenhagen, 1985, p. 40; Phys. Lett. **B** to be submitted
42) E. Hammarén, E. Liukkonen, M. Piiparinen, J. Kownacki, Z. Sujkowski, Th. Lindblad and H. Ryde, Nucl. Phys. **A321** (1979) 71
43) Z. Sujkowski, D. Chmielewska, M.J.A. de Voigt, J.F.W. Jansen and O. Scholten, Nucl. Phys. **A291** (1977) 365
44) W. Nazarewicz, P. Olanders, I. Ragnarsson, J. Dudek and G.A. Leander, Phys. Rev. Lett. **52** (1984) 272; **53** (1984) 2060
45) A.L. Goodman, Nucl. Phys. **A230** (1974) 466